Facies reconstruction from Resistivity-at-the-Bit images recorded in a submarine felsic volcanic succession

Juliane Arnold [a], Anne Bartetzko [b], Gerardo Iturrino [c], Holger Paulick [d]*

a: Applied Geophysics, RWTH Aachen University, 52056 Aachen, Germany

b: Research Center Ocean Margins, University of Bremen. Leobener Strasse, 28359 Bremen, Germany

c: Borehole Research Group, Lamont-Doherty Earth Observatory of Columbia University, Palisades NY, USA

d: Institute of Mineralogy and Petrology, University of Bonn, 53115 Bonn, Germany

**: Corresponding author: Juliane Arnold, phone: +49-241-809 4827, fax: +49-241-809 2132, e-mail address: J.Arnold@geophysik.rwth-aachen.de*

Abstract

For the first time in its history the Ocean Drilling Program (ODP) applied the Logging-While-Drilling (LWD) Resistivity-at-the-Bit (RAB) tool for penetrating into the subseafloor during Leg 193. We focus on ODP Hole 1189C, situated in an active black smoker field within the PACMANUS hydrothermal system (Papua New Guinea) and associated with felsic volcanism in a convergent tectonic setting. Drilling in ODP Hole 1189C proceeded without coring and reached a total depth of 166 meters below seafloor (mbsf). Additional wireline measurements were recorded over an interval of about 50 m. The RAB tool provides electrical images of the borehole wall with lower spatial resolution than the images obtained from the wireline Formation Micro Scanner (FMS) tool but in contrast yields a full 360° coverage of the borehole wall. Due to their higher resolution, FMS images from the same depth range allow calibration of patterns in RAB images. The final interpretation of the RAB images leads to a distinction between coherent dacite and two types of breccias with different clast sizes. Analysis of the RAB images shows that the architecture of the volcanic sequence drilled at ODP Hole 1189C consists of frequently alternating successions of coherent dacite and the two

types of breccia, all hydrothermally altered. RAB data from ODP Hole 1189C are the only source of information of the upper 10s of meters at the Roman Ruins site and show that the near-surface intervals are composed of brecciated dacite. The results were compared with existing models on Pual Ridge volcanic architecture.

Keywords: downhole logging, facies reconstruction, felsic volcanic succession, hydrothermal alteration, Ocean Drilling Program Leg 193, Resistivity-at-the-Bit

Introduction

ODP Leg 193 (Shipboard Scientific Party 2002) was the first in ODP history which was drilled into the active PACMANUS (Papua New Guinea-Australia-Canada-Manus) hydrothermal vent field located in felsic submarine volcanic rocks. This hydrothermal field is situated on the crest of a dacitic volcanic ridge (Pual Ridge). Pual Ridge belongs to a chain of submarine volcanoes in the eastern part of the Manus back-arc basin (Fig. 1). Several previous ODP legs drilled active hydrothermal systems hosted in basaltic volcanic rocks (e.g. Davis et al. 1992; Humphries et al. 1995; Fouquet et al. 1998). They encountered difficult drilling conditions resulting in low core recovery and unstable boreholes. Therefore, a new drilling strategy was used during ODP Leg 193: Several coring, wireline logging and Logging-While-Drilling (LWD) techniques were combined to increase the overall information availability (Binns et al. 2002). In total, six holes deeper than 50 mbsf were drilled at ODP Sites 1188 (Snowcap) and 1189 (Roman Ruins) (Fig.1). Core recovery was poor in all coring holes ranging on average from 6.8-18.3 %. Therefore, information from geophysical downhole measurements is important to understand subseafloor geology at Pual Ridge.

During conventional wireline logging a tool string is lowered into the borehole on a cable and data are recorded while pulling the tool string back to the surface. In contrast LWD integrates modified logging tools as part of the drill string bottom hole assembly. Unlike wireline methods and many coring techniques LWD allows geophysical parameters to be obtained beginning right at sea floor. Core material cannot be recovered through LWD tools employed during ODP Leg 193. The Resisitvity-at-the-Bit (RAB) tool provided complete-coverage electrical images of the borehole wall at three different lateral depths of investigation. ODP Hole 1188B (Snowcap) and Hole 1189C (Roman Ruins) were drilled with the RAB-tool and reached 70 and 166 mbsf, respectively. ODP Hole 1189C is particularly interesting since additional wireline logs were recorded in an overlapping interval of 50 m (Fig. 2). Thus data from these two different downhole logging techniques can be compared and integrated. ODP Leg 193 was the first deployment of the RAB in ODP. It was successfully used later on during Leg 196 (Mikada et al. 2004) and in a modified version allowing “Logging-while-coring” during Legs 204 and 209 (Goldberg et al. 2004). The Integrated Ocean Drilling Program (IODP), successor of the ODP, recently employed the RAB during two expeditions (Expedition 308 and 311 scientists 2005).

Coring in the adjacent ODP Holes 1189A and 1189B, only a few 10 seconds of meters distant from ODP Hole 1189C, showed that volcanic deposits at Roman Ruins include coherent volcanic rocks and volcaniclastic units (Binns et al. 2002; Paulick et al. 2004). Lithostratigraphic reconstructions of the dacitic extrusive sequence drilled at Roman Ruins are based on the limited number of cores (Paulick et al. 2004) and on downhole geophysical data, in particular high-resolution electrical images from the wireline Formation Micro Scanner (FMS) tool (Bartetzko et al. 2003). These studies demonstrated that the drilled succession consists of associations of coherent, volcaniclastic, and brecciated dacite, all strongly hydrothermally overprinted. Fluid-dacite interaction has generated diverse alteration-related textures and mineral assemblages, including anhydrite, pyrite, chlorite, illite and quartz (Binns et al. 2002; Bach et al. 2003).

In this paper we give a detailed interpretation of the RAB data in ODP Hole 1189C with respect to a lithostratigraphical reconstruction. A detailed comparison of the wireline and RAB data provides an important quality check of the data. The facies interpretation presented in this study particularly focuses on the texture of dacite breccia and therefore refines the reconstruction given by Bartetzko et al. (2003). We discuss the results in relation to the volcanic evolution of Pual Ridge and hydrothermal activity at Roman Ruins. These interpretations also illustrate potential applications of LWD-RAB measurements in unstable boreholes where no conventional downhole wireline logs can be used and information from cores is missing or scarce.

Downhole measurements

Downhole logging measurements obtained in ODP Hole 1189C included Logging-While-Drilling RAB data from 0–166 mbsf and wireline data in an interval of 50 m between 10–60 mbsf (Fig. 2). The RAB tool recorded electrical resistivity, electrical borehole images, and natural gamma radiation. In addition, drilling parameters such as rate of penetration and bit rotation were registered. Wireline logs include electrical resistivity, density, photoelectric factor, borehole diameter, total and spectral gamma ray and also high-resolution borehole micro-resistivity images recorded by the Formation MicroScanner (FMS). An overview of the wireline and RAB downhole measurements is shown in Table 1. Principles of wireline logging tools deployed in ODP Leg 193 are described in Borehole Research Group (2002). A short introduction into RAB measurement principles is given below.

Principles of the RAB tool

The RAB tool offers five different measurements of electrical resistivity at different vertical resolution and depth of penetration (Bonner et al. 1996). Figure 3 shows the RAB tool deployed during ODP Leg 193. In this configuration the RAB tool is run on top of the drill bit and provides the following resistivity measurements: (1) The drill bit is used as an electrode and provides the intrinsic Resisitivity-at-the Bit (RAB) curve with a vertical resolution of 60 cm (23.64 inch). Electrical resistivity is measured by feeding a 1.5 kHz alternating current into the formation (Bonner et al. 1996). The current flows back into the drill pipe and drill collars above the transmitter. Formation resistivity is obtained as the ratio of current into the formation and the transmitter voltage. (2) A focused lateral resistivity measurement is obtained using a 3.8 cm (1.5 inch) wide cylindrical (ring) electrode located 91 cm (35.85 inch) above the bottom of the tool. The vertical resolution of this ring measurement is 5 cm. (3-5) Three button electrodes yield azimuthal resistivity at three different depths of penetration during rotary drilling (shallow, BSAV – 27.94 cm (11 inch), medium, BMAV – 38.1 cm (15 inch), and deep, BDAV – 48.26 cm (19 inch). Each of these azimuthal resistivity measurements provides an image of the borehole wall.

A NaI crystal detector (6) below the ring electrode provides a measurement of natural gamma radiation (Bonner et al., 1996). Spectral information on the contributions of Potassium, Thorium and Uranium is not obtained by this tool.

The maximum sampling rate for data acquisition by the RAB is 10 seconds and optimum results are obtained at a rate of penetration of 9m/h (Borehole Research Group 2002). During ODP Leg 193, data was stored downhole in the internal memory of the RAB and related to depth after the tool had been brought back to the rig floor.

Comparison of wireline logs and LWD data

Size and shape of the borehole are unknown for most intervals of ODP Hole 1189C as geometry was only obtained from wireline logging. Caliper logs indicate that the borehole is larger (12–13 inches) than bit size (9.875 inch) over the entire depth interval and locally exceeds 14 inches. Except for a strong enlargement between 26 and 29 mbsf, FMS images are of good quality. Electrical resistivity from RAB and wireline logs varies from 0.4-13.2 Ωm This value range is comparable with measurements from other boreholes drilled during ODP Leg 193 (Binns et al. 2002; Bartetzko et al. 2003). Formation electrical resistivity at PACMANUS is lower than typically observed in volcanic rocks (a few Ωm to several hundred Ωm; Bartetzko et al. 2005; Kajiwara et al. 2005). These low electrical resistivity values at PACMANUS are attributed to abundant fracturing, locally high vesicularity, intense alteration of the rocks and also polarization effects due to the presence of sulfide minerals (Bartetzko et al. 2006). In the overlapping interval (10-60 mbsf), the correlation coefficients r for the deep, medium, and shallow electrical resistivity measurements are 0.62, 0.61 and 0.61, respectively (Fig. 4). The agreement between the different resistivity curves is less than typically observed for electrical resistivity measurements (e.g. Bartetzko et al. 2001; 2005). Variations in rate of penetration may be a factor explaining low correlation between the resistivity curves. The wireline logs were acquired at a constant logging speed while the rate of penetration during LWD operations varied strongly between 1 and 44 m/hr with an average value of 14.5 m/hr, while the optimum value is 9 m/hr (Binns et al. 2002) (Fig. 2). LWD data have to be converted from time to depth first and this is complicated in ODP Hole 1189C by the rapid and irregular rate of penetration. If this is not done vertical resolution of the tools is different and affects correlation. Electrical resistivities at deep and medium depth of investigation are in good agreement in value ranges for both LWD- and wireline-measurements. For the shallowest depth of investigation electrical resistivity values from wireline measurements are higher compared to those recorded by the RAB.

Values of natural gamma radiation are high and have values of up to 258 gAPI (measured by RAB and wireline tools). Potassium, thorium and uranium contents are between 0.6-4.3 wt. %, 0.3-4.6 ppm and 2.5-22.5 ppm, respectively.

Natural gamma radiation between LWD and wireline logs can easily be correlated ($r = 0.76$), but RAB values are mostly lower than wireline values; the average values for measurements by the RAB and the Natural Gamma Ray Spectrometry Tool are 111 and 122 gAPI, respectively, for the interval between 15 and 60 mbsf (Fig. 4). Potential reasons for these differences are the irregular rate of penetration possibly resulting in time windows too short for reliable measurements, as accuracy of natural gamma ray measurements depends on recording time (e.g. Rider 1996).

A comparison of RAB and FMS images from the same depth interval is shown in Figure 5. These resistivity images illustrate the difference in resolution between the two techniques. Wireline FMS images have a vertical resolution of 5 mm, whereas the resolution of RAB images is several cm to a few dm. Thus the FMS image shows small details, like single clasts or fractures whereas the significance of the RAB is to show larger structures. The advantage of the RAB images is that due to the 360° borehole wall coverage, larger features are displayed in their complete shape and not discontinuous as in FMS images.

Identification of volcanic textures using RAB and FMS images and logging data

ODP Hole 1189C was drilled without coring and therefore gathering information on volcanic stratigraphy is one important aspect of geophysical downhole log interpretation in this hole. Investigations of cores and FMS images from the neighboring ODP Holes 1189A and 1189B show that the volcanic facies at Roman Ruins is dominated by dacite breccia, volcaniclastic breccias and coherent dacite (Bartetzko et al. 2003; Paulick et al. 2004). These facies may be identified using FMS images due to their high resolution that allow tiny features to be recognized such as vesicles, single breccia clasts or flow banding. For example, coherent dacite, representing the insulated central part of the lava flow, was identified by a clear fracture pattern in FMS images with many intervals showing small resistive dots which were interpreted as vesicles filled with water or phyllosilicate minerals (Bartetzko et al. 2003). Breccias typically show a characteristic heterogeneous resistivity structure in FMS images. Small resistive features interpreted as clasts are surrounded by a conductive matrix and features such as variations in grain size may give hints to the origin of the breccia (Bartetzko et al. 2003). Facies differentiation is much more difficult using RAB images as small features that may be critical for facies identification are not resolved. The overlapping interval between RAB and wireline logs in ODP Hole 1189C provides the opportunity to calibrate resistivity textures in the electrical images between the high-resolution FMS images and lower resolution RAB images. Bartetzko et al. (2003) showed that the most important facies types occur within this depth interval. Within the RAB intervals, the study by Bartetzko et al. (2003) distinguished only between coherent and brecciated dacite. In this paper, we focus on the interpretation of breccias displayed in the RAB images in order to refine the lithostratigraphic reconstruction of ODP Hole 1189C and provide more information as a basis to understand volcanic evolution of Pual Ridge.

Classification of dacite breccia

Breccias are important constituents of the volcanic stratigraphy at Roman Ruins and make up 40-55 % of the drilled intervals (Bartetzko et al. 2003; Paulick et al. 2004). These breccias may represent primary volcaniclastic material, but they can also be generated by tectonic or hydrothermal processes including fracturing, veining, and in the course of multi-phase hydrothermal alteration (Paulick et al. 2004). Because of these different processes producing breccias at Roman Ruins, additional textural characteristics, such as clast size grading or rotation, as observed in cores at ODP Site 1189, are essential to distinguish between breccias of different origin. Such detailed observations could be obtained from high-resolution FMS data, but can not be resolved in RAB images. Therefore, the term "dacite breccia" was used in a descriptive sense including genuine volcaniclastic rocks and coherent dacite fractured by non-volcanic processes.

By comparing RAB images and FMS images in the overlapping interval, we observed significant differences in resistivity texture of intervals that were classified as dacite breccia. In RAB images, they show a heterogeneous resistivity texture with frequent small-scale changes between conductive and resistive features. Similar to FMS images of breccias, resistive features are surrounded by a conductive matrix. We used the variability in resistive clast size and shape to distinguish two types of dacite breccia in RAB images: Breccia type I with large and irregular resistive clasts and breccia type II with smaller and more regular clasts (Fig. 5). Type I breccias have resistive clasts of 40 to 80 cm in width and 20 to 50 cm in height. They are mostly flat, but irregular forms occur. Type II breccias have smaller resistive clasts that are between 10 and 50 cm in width and 5 to 15 cm in height and are mostly flat. Size of clasts was estimated using the depths of penetration of the three RAB data sets given in the tool specifications to calculate circumference of the images. Numbers of clasts sizes given above are approximate because clasts do not appear as sharp features in the images because of the low resolution, therefore, exact tracing of the outlines of the clasts is not possible. Resistive clast sizes used to differentiate the two types of breccias do not necessarily correspond to real breccia clast sizes. Comparison with FMS images shows that rock clasts are mostly smaller (mostly several cm) than the resistive clasts observed in the RAB images. However, dacite breccia in submarine felsic volcanic successions can preserve clast sizes between 2 mm and 1.2 m across representing in situ and redeposited hyaloclastite or auto breccia, respectively (Stewart and McPhie 2006). Intervals of volcaniclastic material identified in the FMS profile correspond to both types of breccia in the RAB profile, thus, differences in resistivity texture between breccia types I and II do not allow the origin of the breccias to be accounted for. Figure 5 shows resistivity patterns of the three facies for different penetration depths. For the large homogeneous patterns characteristic of coherent dacite, images do not present much difference. The smaller-scale patterns of the breccias, particularly breccia type II, show more variations between the images of different depths of penetration; differences in depth of penetration between the images are larger than the size of single resistive clasts. The two types of breccias do not show differences in electrical resisitvity values; the distinction between the two types is based on textural variations. However, dacite breccia may be distinguished from coherent dacite by slightly lower electrical resistivity values (average value 1.4–1.5 Ωm for the resistivity measured at deep and medium penetration depth in breccias and 2.8–2.9 Ωm in coherent dacite; and by slightly higher natural gamma radiation (105 and 125 gAPI on average for breccia I and II, respectively, and 74 gAPI in coherent dacite; Fig. 6).

Facies interpretation of ODP Hole 1189C

Due to the combination of the RAB tool and wireline logging in ODP Hole 1189C (Leg 193), it was possible to reconstruct a synthetic lithological profile in a hydrothermally altered dacite sequence. The reconstructed lithostratigraphic profile of ODP Hole 1189C based on RAB images is shown in Figure 6 and compared with the FMS-based profile. In the overlapping interval, two coherent units are recognized in the same depth intervals (36–40 mbsf and 50-55 mbsf) in both RAB and FMS images. The second of the two coherent units is thinner in the RAB profile. This unit is characterized by a strongly fractured top which appears as a breccia of type I in the RAB images.

The RAB profile shows that ODP Hole 1189C is characterized by an interlayering of coherent dacite and dacite breccia. Coherent facies units amount to 35.6 % of the reconstructed lithology and range in thickness from 5 m to 31 m. They are concentrated in the lower part of the borehole. Two thin, 1-m thick layers of breccia type I interrupt the thickest coherent unit (77 to 108 mbsf). A similar small breccia layer within a coherent dacite unit was also observed in FMS images of the neighboring ODP Hole 1189B (Bartetzko et al. 2003).

In the overlapping interval, where the volcaniclastic facies was identified from normal grading in FMS images, alternating bedding of breccias type I and II is observed in RAB images. However, RAB images do not allow grading in clast size to be identified. Alternating sequences of different breccia occur in several other intervals, e.g. between 115 and 137 mbsf and between 0 and 27 mbsf. Resistivity texture of the breccias changes over intervals of 1 to 5 m in thickness.

Formation electrical resistivity is low in all of the ODP Leg 193 boreholes (0.07–13.20 Ωm) in which formation resistivity values measured in ODP Hole 1189C (0.23-13.20 Ωm) are in the range of the higher resistivity values. Higher values > 10 Ωm occur in several discrete intervals within the coherent dacite units between 76 and 115 mbsf. The higher electrical resistivity values within this interval indicate that these coherent units are less fractured and altered than the remaining intervals of the hole. This is confirmed by lower gamma ray values (down to 34 gAPI, on average 70 gAPI). The four coherent units are separated by thin brecciated intervals, which are characterized by low electrical resistivity and high gamma ray values (Fig. 6). These physical properties indicate stronger fracturing and alteration in connection with an enrichment of radioactive elements.

The facies association encountered in the reconstructed lithological profile of ODP Hole 1189C contains large proportions of brecciated material (breccia type I: 39.9 % and breccia type II: 24.5 %). The small proportion of coherent facies (36 %) and frequent facies changes in ODP Hole 1189C, confirm that the borehole is located in an intermediate position between proximal and distal facies associations with respect to the volcanic vent (De Rosen-Spence et al. 1980; Allen 1992; Cas, 1992, Bartetzko et al. 2003; Paulick et al., 2004). All in all, those frequently alternating successions of coherent dacite and dacite breccia are typically common in felsic volcanic complexes (Stewart and McPhie 2006).

LWD data from ODP Hole 1189C are the only source of information for the uppermost 10s of meters at Roman Ruins. Core recovery is extremely poor in the upper part of ODP Hole 1189A (< 5 %) and coring and downhole logging started at 30 and 40 mbsf in ODP Hole 1189B. The uppermost intervals are particularly interesting at PACMANUS. At the Snowcap Site (1188), a low temperature venting field about 800 m from Roman Ruins, a 35 m thick cap of fresh dacite rocks overlying the strongly altered formation was observed in core and downhole logging data (Binns et al. 2002; Bartetzko et al. 2003; Paulick et al. 2004). This layer of fresh dacite may be of importance for fluid circulation patterns at the Snowcap site. LWD data do not indicate the presence of any fresh or coherent dacite layers within the uppermost 40 m of ODP Hole 1189C, but show the typical resistivity texture of breccias in the RAB images. Electrical resistivity values are low compared to the thick coherent intervals between 76 and 115 mbsf. High gamma ray values of up to 190 gAPI indicate a strong alteration. We therefore conclude that a similar structure with a fresh capping rock as found at the Snowcap site does not exist at Roman Ruins.

Conclusions

Deriving lithostratigraphical information from ODP Hole 1189C is particularly challenging due to the lack of cores, the low resolution of the RAB images and the restriction to only two physical properties (electrical resistivity and natural gamma radiation) for most intervals of the hole. FMS images in the overlapping interval of ODP Hole 1189 C and knowledge of facies association derived from cores from the neighbouring holes was essential for the identification of volcanic facies in RAB images. We were able to establish a lithostratigraphical profile that is suitable to test existing models on subsurface geology of the region. Due to the rapid lateral changes that are typical for submarine felsic volcanic sequences, RAB data from ODP Hole 1189C provide important additional information on the Roman Ruins site. Although we were able to identify two different types of breccias, resolution of the RAB images is insufficient to allow any interpretation of their origin which could be essential for a more profound understanding of their origin. The interpretation based on electrical resistivity and natural gamma radiation allows variations in structure and alteration of the rocks to be distinguished. ODP Hole 1189C is the only hole at the Roman Ruins site where continuous information on the uppermost tens of meters of the borehole is available and thus the lithostratigraphy can be acquired. Our results from ODP Hole 1189C show that, unlike the situation at the Snowcap site, a cap of fresh dacites does not exist at the Roman Ruins site. Detailed studies of RAB images were crucial for identifying structures in this hydrothermally altered felsic volcanic complex since wireline logging was impossible over most intervals of the hole due to borehole wall collapse resulting in total blockage of the borehole.

References

Allen, R. L. (1992) Reconstruction of the tectonic, volcanic, and sedimentary setting of strongly deformed Zn-Cu massive sulfide deposits at Benambra, Victoria. *Econ. Geol., 87*, pp 825-854

Bach, W., Roberts, S., Vanko, D. A., Binns, R. A., Yeats, C. Y., Craddock, P., and Humphris, S. E. (2003) Controls of fluid chemistry and complexation on REE contents of anhydrite from the Pacmanus subseafloor hydrothermal system, Manus Basin, Papua New Guinea, *Min. Dep.*, 38, pp 916-935

Bartetzko, A., Pezard, P., Goldberg, D., Sun, Y.-F., and Becker, K. (2001) Volcanic stratigraphy of DSDP/ODP Hole 395A: An interpretation using well-logging data. Mar. Geophys. Res. 22: 111-127

Bartetzko, A., Klitzsch, N., Iturrino, G.J., Kaufhold, S., and Arnold, J. (2006) Electrical properties of hydrothermally altered dacite from the PACMANUS hydrothermal field (ODP Leg 193). *Journal of Volcanology and Geothermal Research*, 152, pp 109-120

Bartetzko, A., Paulick, H., Iturrino, G., and Arnold, J. (2003) Facies reconstruction of a hydrothermally altered dacite extrusive sequence – evidence from geophysical downhole logging data (ODP Leg 193). *Geochemistry, Geophysics, Geosystems*, 4 (10), doi: 10.1029/2003GC000575

Bartetzko, A., Delius, H., and Pechnig, R. (2005) Effect of compositional and structural variations on log responses of igneous and metamorphic rocks I: mafic rocks. In: Harvey, P.K., Brewer, T.S., Pezard, P.A., and Petrov, V.Y. (Eds.) *Petrophysical properties of crystalline rocks.* Geological Society Special Publications. 240, pp 255-278

Binns, R. A., Barriga, F. J. A. S., Miller, D. J, and Ocean Drilling Program Leg 193 Shipboard Scientific Party (2002) *Proceedings of the Ocean Drilling Program, Initial Reports*, vol. 193, Ocean Drill. Program, College Station TX. (CD-ROM, available from: Ocean Drilling Program, Texas A&M University, College Station TX 77845-9547, USA)

Bonner, S., Fredette, M., Lovell, J., Montaron, B., Rosthal, R., Tabanou, J, Wu, P., Clark, B., Mills, R., & Williams, R. (1996) Resistivity While Drilling - Images from the String. *Oilfield Rev*., 8, pp 4-19

Borehole Research Group, ODP Logging Manual (2002) An electronic guide to ODP Logging services, [CD-ROM] Lamont-Doherty Earth Observatory, Palisades, NY. (http://www.ldeo.columbia.edu/BRG/ODP/LOGGING/MANUAL/index.html).

Brewer, T.S., Harvey, P.K., Lovell, M.A., Haggas, S., Williamson, G. and Pezard, P. (1998) Ocean floor volcanism: constraints from the integration of core and downhole logging measurements. In: Harvey, P.K. and Lovell, M.A. (eds.) Core-Log Integration. Geological Society, London, Special Publications. 136, pp 341-362

Cas, R.A.F. (1992) Submarine Volcanism: Eruption styles, products, and relevance to understanding the host-rock successions to volcanic-hosted massive sulfide deposits. *Economic Geology*. 87, pp 511-541

Davis, E. E., Mottl, M. J., Fisher, A. T., and Ocean Drilling Program Leg 139 Shipboard Scientific Party (1992) *Proceedings of the Ocean Drilling Program, Initial Reports, vol. 139,* Ocean Drill. Program, College Station TX

De Rosen-Spence, A.F., Provost, G., Dimroth, E., Gochnauer, K., and Owen, V. (1980) Archean subaqueous felsic flows, Rouyn-Noranda, Quebec, Canada, and their Quaternary equivalents. *Precam. Res*., *12*, pp 43-77

Expedition 308 Scientists (2005) Overpressure and fluid flow processes in the deepwater Gulf of Mexico: slope stability, seeps, and shallow-water flow. *IODP Prel. Rept*., 308. doi:10:2204/iodp.pr.308.2005

Expedition 311 Scientists (2005) Cascadia margin gas hydrates. IODP Prel. Rept., 311. doi:10:2204/iodp.pr.311.2005

Fouquet, Y., Zierenberg, R. A., Miller, D. J., and Ocean Drilling Program Leg 169 Shipboard Scientific Party (1998) *Proceedings of the Ocean Drilling Program, Initial Reports, vol. 169*, Ocean Drill. Program, College Station TX

Goldberg, D., Myers, G., Iturrino, G., Grigar, K., Pettigrew, T., Mrozewski, S., and Shipboard Scientific Party, ODP Leg 209 (2004) Logging-While-Coring – First Tests of a New Technology for Scientific Drilling. Petrophysics, 45: 328-334

Humphries, S. E., Herzig, P. M., Miller, D. J., and Ocean Drilling Program Leg 158 Shipboard Scientific Party (1995) *Proceedings of the Ocean Drilling Program, Initial Reports, vol. 158*, Ocean Drill. Program, College Station TX.

Kajiwara, T., Ikeda, R., Nakada, S., Uto, K., and Nishi, M. (2005) Unzen volcano scientific drilling: well logging data of the USDP-4. International Workshop on Unzen Scientific Drilling Project (USDP), Shimabara, Nagasaki, Japan, 26-28 February 2005

Mc. Phie, J., Doyle, M., and Allen, R. (1993) *Volcanic textures – A guide to the interpretation of textures in volcanic rocks*, Centre for Ore Deposit and Exploration Studies, University of Tasmania, 198 pp

Mikada, H., Becker, K., Moore, J.C., Klaus, A., et al. (2002) Proc. ODP, Init. Repts., 196 [CD-ROM]. Available from: Ocean Drilling Program, Texas A&M University, College Station TX 77845-9547, USA

Paulick H., Vanko, D. A., and Yeats, C. J. (2004) Drill core-based facies reconstruction of a deep-marine, felsic volcano hosting an active hydrothermal system (Pual Ridge, Papua New Guinea, ODP Leg 193), *J. Volcanol. Geotherm. Res*. 130, pp 31-50

Rider, M. H. (1996) *The geological interpretation of well logs*, Whittles Publishing, Caithless, 288 pp

Shipboard Scientific Party (2002) Proceedings of the Ocean Drilling Program, Initial Reports, 193, College Station, USA.

Stewart, A. L. and McPhie, J. (2006) Facies architecture and Late Pliocene – Pleistocene evolution of a felsic volcanic island, Milos, Greece. *Bull. Volcanol.*, 68, pp 703-726

Figure captions

Figure1. (a) Tectonic configuration of the Manus back-arc basin (arrows indicate direction of plate movement) and bathymetric map of the PACMANUS hydrothermal vent field located on the crest of the volcanic Pual Ridge (Leg 193 drilling sites 1188 and 1189 are inserted). Bathymetry is expressed in meter below sealevel (after Binns et al., 2002). (b) Coring and logging program of Site 1189 Holes A, B and C. The numbers below the boreholes are the average core recovery and mbsf is defined as meters below seafloor.

Figure 2. Composite log of Hole 1189C (Roman Ruins). Abbreviations: RAB: Resistivity-At-the-Bit; FMS: Formation MicroScanner; C1 and C2: FMS caliper; ROP: Rate of Penetration, BDAV: deep average button resistivity log; BMAV: medium average button resistivity log; BSAV: shallow average button resistivity log; IDPH: deep induction electrical resistivity log, IMPH: medium induction electrical resistivity log; SFLU: shallow spherically focused resistivity; GR and SGR: total gamma ray logs. Wireline logs range from ~ 10 mbsf to 60 mbsf, whereas LWD data are recorded from ~ 0 mbsf to 160 mbsf.

Figure 3. A schematic diagram showing the configuration of the LWD RAB tool that was used to drill Hole 1189C: (1) drill bit; (2) ring electrode; (3–5) three azimuthal button electrodes; they rotate with the entire bottom-hole assembly scanning the borehole wall and recording a full 360° coverage image directly behind the drill bit; (6) NaI crystal detector (modified after Binns et al., 2002).

Figure 4. Crossplots of electrical resistivity and gamma-ray measurements from LWD (BDAV, GR) and wirline logging (IDPH, SGR) for the overlapping interval (~ 10 – 60 mbsf).

Figure 5. Examples of volcanic facies identified in RAB images from Hole 1189C. RAB images are available from three distinct depths of investigation: shallow (28 cm), medium (38

cm) and deep (48 cm). FMS images are shown from the same depth intervals. All images are dynamically processed. The orientation is given above in ° with respect to North. RAB images allow to distinguish between coherent dacite and two types of breccia (breccia type I and breccia type II). Whereas the shape of structural features, marked with black lines, are hardly changing in units of coherent dacite, the smaller-scale patterns of the breccias show more variations between the images of different depths of penetration.

Figure 6. Results obtained from the volcanic facies reconstruction using logging data from Hole 1189C. On the left hand side relevant curves for the log interpretation are shown. These are: electrical resistivity logs in logarithmic scale (deep (BDAV), medium (BMAV), shallow (BSAV) average button resistivity logs) and the total gamma ray log (GR). At the right side the result of RAB image interpretation is presented and compared to the profile from FMS image interpretations.

Figures and Table

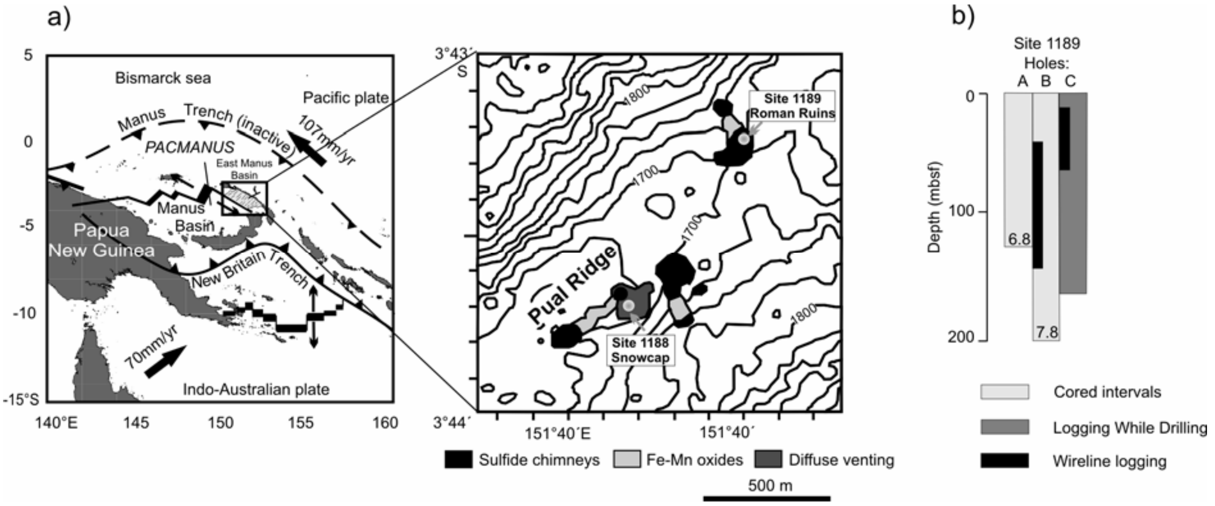

Figure1.

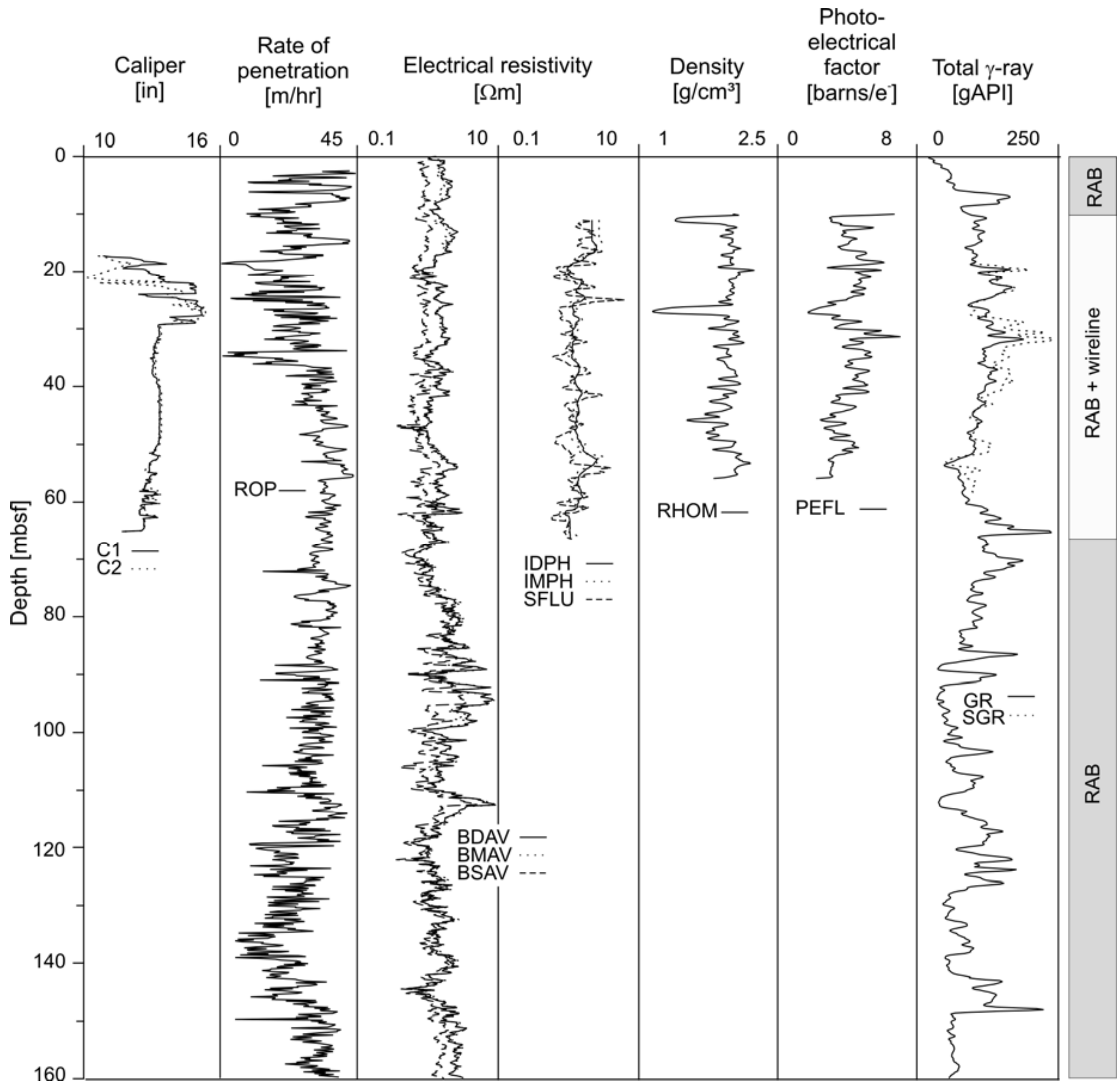
Caliper
[in]
10
16
Rate of
penetration
[m/hr]
0
45
Electrical resistivity
[Ωm]
0.1
10
0.1
10
Density
[g/cm³]
1
2.5
Photo-
electrical
factor
[barns/e-]
0
8
Total γ-ray
[gAPI]
0
250
Depth [mbsf]
0
20
40
60
80
100
120
140
160
C1
C2
ROP
IDPH
IMPH
SFLU
BDAV
BMAV
BSAV
RHOM
PEFL
GR
SGR
RAB
RAB + wireline
RAB

Figure 2.

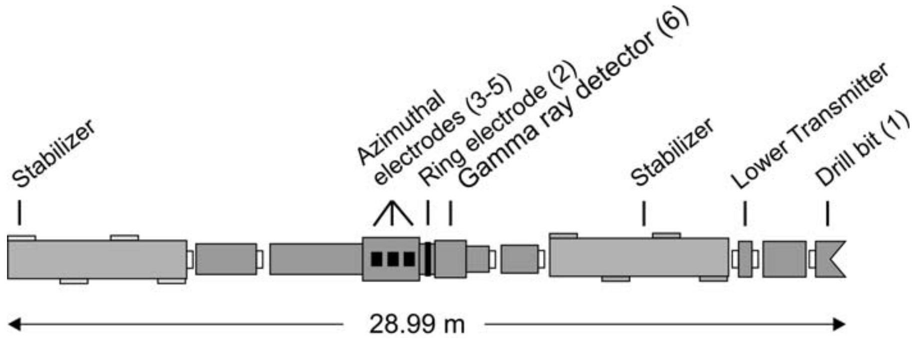
Stabilizer
Azimuthal
electrodes (3-5)
Ring electrode (2)
Gamma ray detector (6)
Stabilizer
Lower Transmitter
Drill bit (1)
28.99 m

Figure 3.

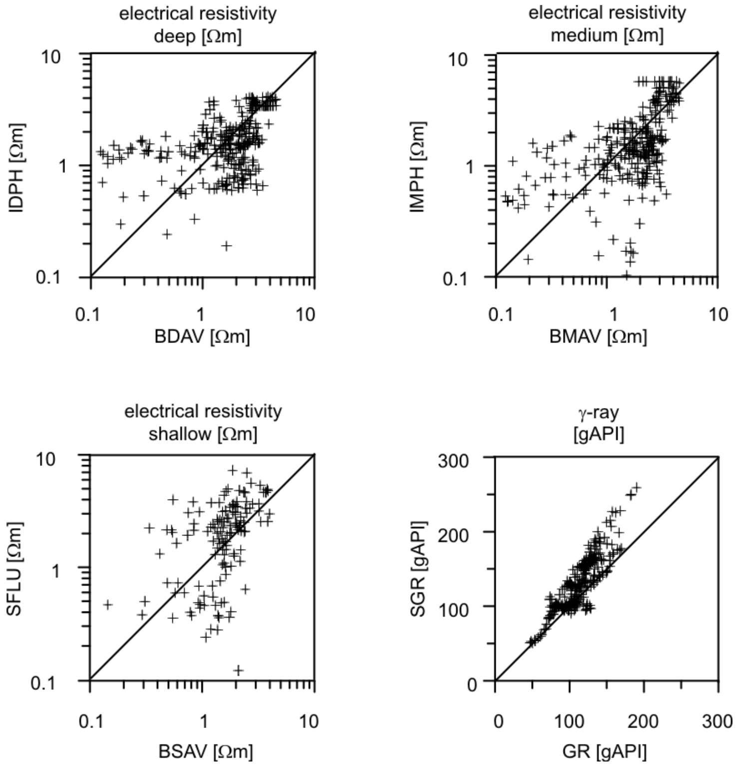

electrical resistivity
deep [Ωm]
10
1
0.1
IDPH [Ωm]
0.1
1
10
BDAV [Ωm]
electrical resistivity
medium [Ωm]
10
1
0.1
IMPH [Ωm]
0.1
1
10
BMAV [Ωm]
electrical resistivity
shallow [Ωm]
10
1
0.1
SFLU [Ωm]
0.1
1
10
BSAV [Ωm]
γ-ray
[gAPI]
300
200
100
0
SGR [gAPI]
0
100
200
300
GR [gAPI]

Figure 4.

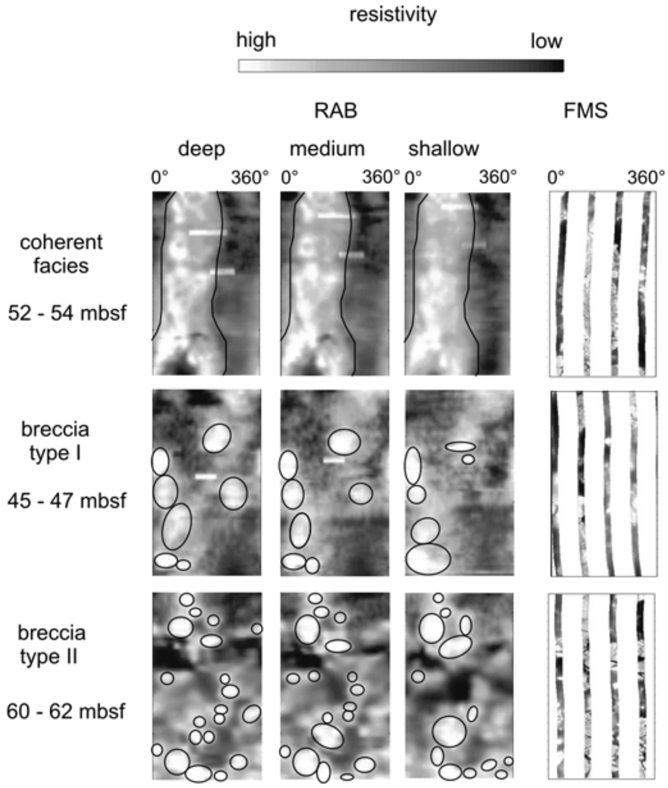
resistivity
high
low
RAB
FMS
deep
medium
shallow
0°
360°
0°
360°
0°
360°
0°
360°
coherent facies
52 - 54 mbsf
breccia type I
45 - 47 mbsf
breccia type II
60 - 62 mbsf

Figure 5.

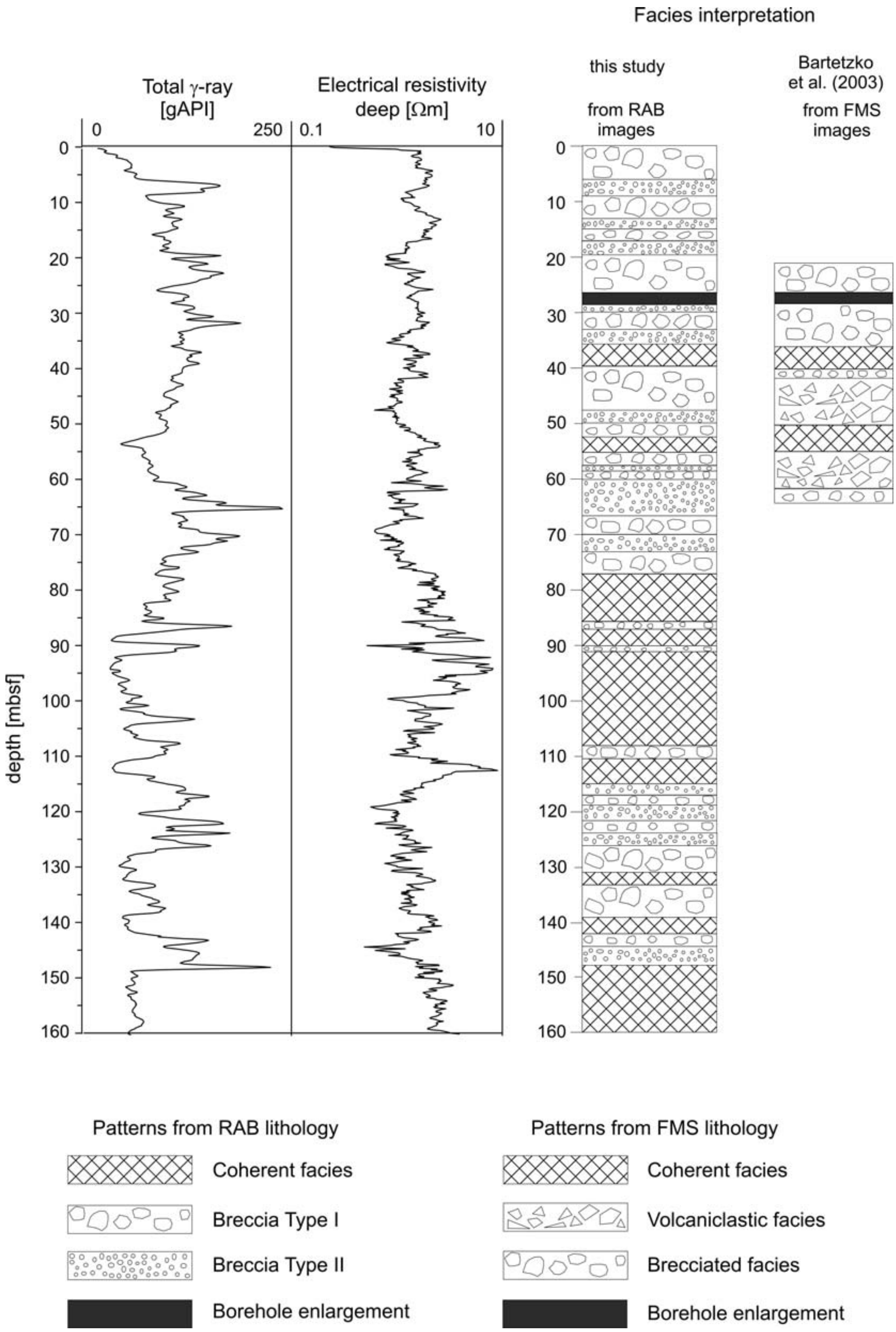

Facies interpretation
this study
from RAB images
Bartetzko et al. (2003)
from FMS images
Total γ-ray [gAPI]
0
250
Electrical resistivity deep [Ωm]
0.1
10
depth [mbsf]
0
10
20
30
40
50
60
70
80
90
100
110
120
130
140
150
160
Patterns from RAB lithology
Coherent facies
Breccia Type I
Breccia Type II
Borehole enlargement
Patterns from FMS lithology
Coherent facies
Volcaniclastic facies
Brecciated facies
Borehole enlargement

Figure 6.

Table 1. Tools and logs used to reconstruct the lithostratigraphy of Hole 1189C.

Tool	*Logs*		*Method*
	Electrical formation resistivity		
DITE™ (Phasor Dual Induction Tool)	IDPH (Ωm)	Phasor Induction Log Deep	wireline
	IMPH (Ωm)	Phasor Induction Log Medium	
SFL™ (Spherically Focused Log)	SFLU (Ωm)	Spherically Focused Log	
RAB[An] (Resistivity At the Bit)	BDAV (Ωm)	Deep Resistivity Average	LWD
	BMAV (Ωm)	Medium Resistivity Average	
	BSAV (Ωm)	Shallow Resistivity Average	
	RING (Ωm)	Ring Resistivity	
	RBIT (Ωm)	Bit Resistivity	
	RAB images		
FMS™ (Formation Micro Scanner)	FMS images		wireline
	Natural radioactivity		
NGT™ (Natural Gamma Ray Spectrometry Tool)	SGR (API)	total gamma ray	wireline
	CGR (API)	computed gamma ray	
	POTA (wt.%)	potassium content	
	THOR (ppm)	thorium content	
	URAN (ppm)	uranium content	
RAB[An]	GR (API)	total gamma ray	LWD
	Induced radioactivity		
HLDS™ (Hostile-Environment Litho-Density Sonde)	RHOM (g/cm³)	bulk density	wireline
	PEFL (barns/e$^-$)	photoelectric factor	
	LCAL (in)	hole diameter	
	Mechanic and Drilling Parameters		
FMS™	C1, C2 (in)	hole diameter	wireline
RAB[An]	ROP (m/hr)	Rate of penetration	LWD

™ Trademark of Schlumberger Ltd.
[An] Anadrill